Application of vector beams for enhanced high-order harmonics generation in laser-induced plasmas

MOTTAMCHETTY VENKATESH,[1,2,7] RASHID A. GANEEV,[3,4,5,8] ID
VYACHESLAV V. KIM,[3] GANJABOY S. BOLTAEV,[5] ID IBROKHIM B. SAPAEV,[5] JINGGUANG LIANG,[1,6] ID JIAQI YU,[1] AND WEI LI[1,9] ID

[1]*GPL, State Key Laboratory of Applied Optics, Changchun Institute of Optics, Fine Mechanics and Physics, Chinese Academy of Sciences, Changchun 130033, China*
[2]*Department of Materials Science and Engineering, Uppsala University, Box 35, SE-751 03 Uppsala, Sweden*
[3]*Laboratory of Nonlinear Optics, Institute of Astronomy, University of Latvia, LV-1004, Riga, Latvia*
[4]*Department of Physics, Voronezh State University, Voronezh 394006, Russia*
[5]*Tashkent Institute of Irrigation and Agricultural Mechanization Engineers, National Research University, Kori Niyozov street 39, Tashkent 100000, Uzbekistan*
[6]*University of Chinese Academy of Sciences, Beijing 100049, China*
[7]*venkatesh.montamchetty@angstrom.uu.se*
[8]*rashid.ganeev@lu.lv*
[9]*weili1@ciomp.ac.cn*

Abstract: High-order harmonics driven by phase- and polarization-structured femtosecond pulses are unique sources of the extreme ultraviolet vortex and vector beams, which have various applications. Here, we report the generation of intense high-order harmonics during propagation of the polarization-structured vector beams (radially polarized beam, azimuthally polarized beam, and their superposition) through the laser-induced plasmas (In, C, CdS, Zns, Ag_2S). Low-order harmonics became stronger with radially polarized and azimuthally polarized driving beams compared with the linearly polarized beams, which is explained on the basis of phase matching and specific properties of vector beams. Contrary to that, the resonance-enhanced harmonic generated in the indium plasma in the case of radially polarized and azimuthally polarized beams was twice weaker compared with the harmonic generated by the LP beam due to modification in the resonant transition selection rules leading to a decrease of the oscillator strength of ionic transitions. Harmonic cut-off and intensity in the case of superposition of the radially and azimuthally polarized beams were lesser compared with the cases of the individual (radially polarized and azimuthally polarized) beams.

1. Introduction

Coherent extreme ultraviolet light sources are proven to be the useful tools for the investigation of the structural and dynamical properties of matter [1–3]. The extreme ultraviolet sources based on the high-order harmonics generation (HHG) have many attractive characteristics like ultrashort pulse duration, exceptional coherence, tabletop sizes, broad bandwidth, and wide tunability as compared with other sources like X-ray lasers, synchrotron, and free-electron lasers. Intense harmonics are crucial for attosecond science. However, the efficiency of HHG is restricted by the absorbance of harmonics in the generating media and the phase mismatch between the harmonics and fundamental laser field. To overpass this obstacle, several methods like quasi-phase matching, resonance-induced enhancement, and multiparticle media applications have been proposed to generate intense harmonics with higher cut-off energy [4–15].

In recent years, the attention has been increased to generate high-order harmonics having different ellipticities of polarization, especially harmonics with phase and polarization singularities, which is expected to be useful for probing magnetic materials, extreme ultraviolet lithography, ultrafast diffraction imaging, and controlling the orbital angular momentum dichroism of materials etc. [16–19]. Usually, two methods are used for the generation and manipulation of polarization properties of extreme ultraviolet beams: (i) X-ray optics is used to manipulate the generated extreme ultraviolet radiation, and (ii) optical schemes are employed to modulate the emission and obtain structured extreme ultraviolet beams. However, the first method is extremely inefficient, since it requires high-quality X-ray optics and is limited to the narrow bandwidth.

HHG is a highly non-perbutative process. Hence, an efficient way to modify and/or control the polarization of extreme ultraviolet beams generated via HHG is by using the driving pulses of varying polarization (i.e. second method). However, the harmonic intensity decreases with the growth of the ellipticity of driving pulses polarization, and its value almost entirely drops in the case of circular polarized driving pulses due to the drastic decrease of the cross-section of recombination of the accelerated electrons with its parent ion. This limitation is circumvented for generating extreme ultraviolet beams with various polarization singularities by using bi-chromatic counter-rotating circularly polarized fields, two color collinear orthogonally polarized, non-collinear single color counter-rotating circularly polarized driving pulses, etc. [20–26]. These techniques use complicated experimental schemes. Alternatively, the high-order harmonics with circular polarization are produced using spatially structured driving pulses by employing liquid crystals [27]. This scheme produces intense and high-cut-off harmonics compared to the time-structured driving pulses because of higher fraction of fundamental pulse energy is utilized for HHG. Additionally, this approach allows maintaining the precise control over the spatial properties of harmonics.

The effect of spatially- and polarization-variable driving pulses on the intensity and polarization of generated high-order harmonics is reported in Refs. [28] and [29]. It was demonstrated that the circularly polarized even and odd harmonics can be produced in the gas medium by varying the beam waist of the tightly focused radially polarized (RP) driving beam. The tightly focused RP beams generated intense harmonics compared to the azimuthally polarized (AP) and spiral polarized beams. Moreover, harmonics with non-zero angular momentum (i.e., optical vortices) are generated using the non-uniform spatial beams. Hence, the driving pulses with spatially variable polarization (i.e., vector beams) can be useful to generate and control the harmonics of varying polarization representing the elliptical, circular, vector, and vortex extreme ultraviolet beams.

Recently, argon gas and fused silica were used for HHG experiments to generate RP and AP extreme ultraviolet beams [30,31]. Meanwhile, the lower-order harmonic yields from gases and solids are smaller compared to the high-order harmonics produced in laser-induced plasmas. The conversion efficiencies of high-order harmonics and resonant harmonic produced from laser-induced plasmas reached 10^{-5} and 10^{-4}, respectively [9,32]. Many aforementioned applications require the high intense structured extreme ultraviolet beams. Recently, intense harmonics carrying orbital angular momentum (i.e., harmonic vortices) were produced from laser-induced plasmas using the vortex fundamental beams [33]. Alternatively, one can assume that laser-induced plasmas can serve as a medium to generate high flux extreme ultraviolet vector beams via HHG driven by vector laser pulses, which allows the study of the effect of vector driving pulses on the harmonic yield and cut-off.

In this paper, we utilize the vector beams to generate intense harmonics from laser-induced plasmas produced on the surfaces of different targets (cadmium sulfide, carbon, and indium). We study the variation of harmonic yield and cut-off by controlling the polarization of vector beams (RP, AP, and their superposition), as well as evaluate these parameters with the driving pulses having time-variant polarization. The efficiency of harmonic yield and cut-off from

the aforementioned ablated materials is analyzed by modulating the ellipticity of the driving pulses. These studies based on the application of vector driving pulses for HHG in laser-induced plasmas demonstrate the path to achieve intense extreme ultraviolet vector beams for applications in different fields like laser machining, particle acceleration, microscopy, and spectroscopy [18,34–36].

2. Experimental schematic

The experimental layout of HHG in laser-induced plasmas is shown in Fig. 1(a). The femtosecond (fs) pulses from Spitfire Ace laser (Spectra-Physics; 800 nm, 40 fs, 1 kHz) were used as heating pulses and driving pulses in the experiment. The heating pulses were focused on the target using a 300 mm spherical focal lens to create laser-induced plasmas. The driving pulses were delayed with respect to heating pulse by 73 ns using the optical delay line, which is sufficient to observe high-order harmonics from the laser-plasma. The driving pulses after delay line propagate through the polarizer (not shown in Fig. 1(a)) to allow only a specific polarization, i.e. *p*- polarized light.
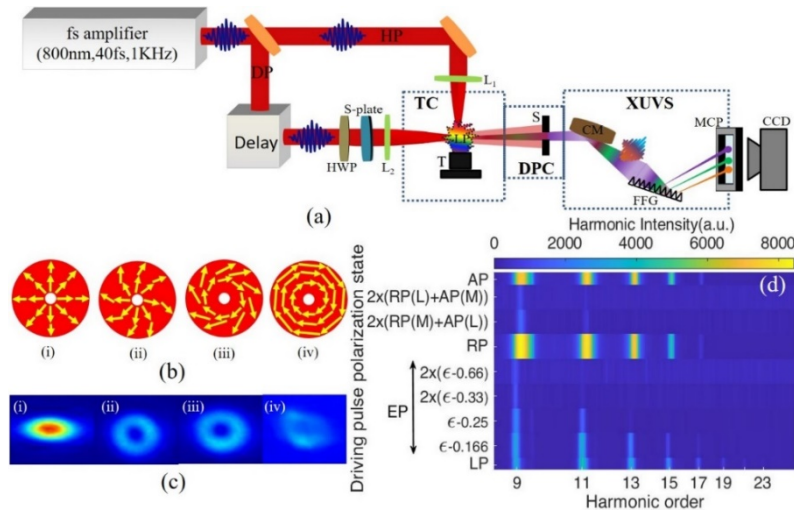

Fig. 1. (a) Experimental setup for high-order harmonics generation. DP: driving pulses; HP: heating pulses; L1,2: focusing lenses for HP and DP, respectively; TC: target chamber; T: target; LP: laser plasma; S: slit; DPC: differential pump chamber; XUVS: extreme ultraviolet spectrometer; CM: cylindrical gold-coated mirror; FFG: flat-field grating; MCP: micro-channel plate; CCD: CCD camera; S-plate: S-wave plate; HWP: half-wave plate; Delay: optical delay line. (b) Various states of light polarization using S-wave plate across the beam cross section. (i) Radial polarization (RP), (iv) Azimuthal polarization (AP), (ii) and (iii) The superposition's of RP and AP. (c) CCD images of (i) linear polarized (LP) Gaussian laser beam, (ii) RP, (iii) AP light at 800 nm, and (iv) AP light at 266 nm (third harmonic of 800 nm radiation). (d) 2d color plots of harmonic spectra showing the influence of the driving pulse polarization on the harmonic intensity and cut off obtained from the carbon plasma (EP: elliptical polarization, RP(M/L)+AP(L/M): laser polarization superposition's having more radial and less azimuthal components and vice versa.

The different states of polarization were obtained by propagating the P-polarized light through the combination of half-wave plate and S-waveplate (RPC-0800-06, Altechna) designed for the 800 nm wavelength. The S-waveplate converts linearly polarized (LP) light into RP and AP when polarization is parallel and perpendicular to the optical axis of the plate, respectively. The corresponding polarization states are shown in Figs. 1(b)[(i) and (iv)]. When light polarization

direction has another angle with respect to the waveplate axis (i.e. 30° and 60°), it allows creating a combination of RP + AP light as illustrated in Figs. 1(b)[(ii) and (iii)] [37]. The obtained state of polarization shown in Fig. 1(b)[(ii)] has more radial components as compared to azimuthal ones. The vice versa condition is shown in the case of Fig. 1(b)[(iii)]. Notice that the percentage of minority components in each superposition is the same.

These polarization states of driving pulses were used to generate high-order harmonics by propagating through different laser-induced plasmas. Heating pulse created laser-induced plasmas while driving pulses generated high-order harmonics by focusing inside the laser plasma from the orthogonal direction using a 500 mm focal length spherical lens. The target position was varied with respect to the optical axis of driving pulses to achieve the maximal harmonic yield. We narrowed our driving pulses down to the diameter of S-waveplate (6 mm), which allowed enhancing the harmonic yield [38].

The harmonics were analyzed in the extreme ultraviolet spectrometer, which consisted of a gold-coated cylindrical mirror, a 1200 lines/mm flat field grating with variable line spacing (Hitachi), a microchannel plate (Hamamatsu), and a CCD camera. The signal present on the microchannel plate phosphor screen was imaged by a CCD camera (Thorlabs) to acquire information on the harmonic intensity and spectral distribution along the extreme ultraviolet region.

Cadmium sulfide (CdS), zinc sulfide (ZnS), silver sulfide (Ag_2S), carbon (C), and indium (In) (all Sigma-Aldrich) were used as the targets for laser-induced plasmas formation and generation of high-order harmonics. We analyzed the effect of state of polarization, as well as the influence of driving pulses ellipticity, on the harmonic intensity and cut-off order using a quarter-wave plate (not shown in Fig. 1(a)). Figures 1(c) (i), (ii), and (iii) show the images of LP, RP, and AP laser beams at λ=800 nm obtained using S-waveplate, while (iv) shows the image of the third harmonic (λ=266 nm) produced in air by AP 800 nm pulses detected using CCD camera. The two-dimensional color plots of high-order harmonics generated from C as the functions of laser polarization are presented in Fig. 1(d). The analysis of these extreme ultraviolet spectra is described in the next section.

3. Results and discussion

3.1. HHG using vector beams

In the HHG process, the electron leaves the parent atom by gaining the energy from the driving pulses. Subsequently, it accelerates and recombines with the parent ion, while converting the gained energy into high-order harmonics. The emitted harmonic intensity and cut-off are strongly affected by the fundamental pulse polarization. The generated intense harmonics having various polarizations like spatially inhomogeneous polarization are a useful source for imaging and spectroscopic studies. The light beams with spatially inhomogeneous polarization are called vector beams. At each point of beam cross-section, the electric field polarization is linear and its vector has spatial dependence (i.e. oriented in different directions) as in Fig. 1(b). RP, AP, and their combinations represent different polarization states of vector beams.

As it was mentioned, RP and AP beams have applications in different fields [18,34–36]. These vector beams can generate intense second, third, and higher-order harmonics due to their peculiar electromagnetic properties [28–30,39–41]. One can anticipate the generation of higher-order harmonics from laser-induced plasmas using such beams. This assumption motivated us to perform the HHG experiments to generate intense coherent extreme ultraviolet radiation driven with AP and RP beams, as well as their superposition, in the case when C, CdS, and In are used as the target materials for laser-induced plasmas formation. We applied the In and C plasmas to study the effect of heterogeneous polarization on the resonant harmonic and overall set of high-order harmonics, respectively. We also studied the CdS plasma to reveal the impact of different vector beams on harmonic generation. In semiconductors, HHG spectroscopy unveils

the effect of resonance phenomenon on some harmonic orders and the clusters influence on harmonic yield [41]. Here we study CdS plasma to reveal the impact of vector beams on harmonic generation. Notice that this is the first report on high-order harmonics emission from the CdS laser-induced plasmas produced on the bulk target.

In our HHG experiments, the heating pulse and driving pulses intensities in the focal planes were 1×10^{15} W/cm^2 and 4.7×10^{14} W/cm^2, respectively. The heating pulse was defocused with respect to the target surfaces to decrease the probability of craters formation. The threshold intensity of laser required to ionize the electron from the nucleus is determined as barrier suppression intensity and defined as 3.8×10^9 I_P^4/Z^2, where I_P is the ionization potential and Z is the ionic atomic number. The I_P of neutral atoms (and singly-charged ions) of C, CdS and In are 11.25 eV (24.38 eV), 7.26 eV (15.62 eV for Cd+) and 5.79 eV (18.86 eV), respectively. C has the highest I_P among the selected targets and the calculated barrier suppression intensities for C and C+ are determined to be $\sim 6 \times 10^{13}$ W/cm^2 and $\sim 3.5 \times 10^{14}$ W/cm^2, which are lower than the employed laser intensities during HHG experiments. Therefore, the used driving pulses are sufficient to produce harmonics from the neutrals and ions contained in laser-induced plasmas.

The high-order harmonics spectra from the aforementioned LIPs are depicted in Fig. 2. The harmonic cut-offs from In, CdS, and C laser-induced plasmas are extended up to 33H (51.1 eV), 25H (38.7 eV) and 25H (38.7 eV) respectively with LP driving pulses. The observed plateau regions of harmonics for CdS, In, and C laser-induced plasmas were 11H-17H, 17H-23H, and 13H-17H, respectively. The generated harmonic cut-offs from laser-induced plasmas of C and In are consistent with previously reported results [33,42]. The harmonic cut-off from CdS is similar to C whereas its harmonic yield is larger with regard to C and In laser-induced plasmas except resonant harmonic in the latter case. Therefore, CdS semiconductor can be considered as a promising material for intense harmonic generation, which might be due to the influence of nonlinear optical properties of sulfide ion present in CdS [43].
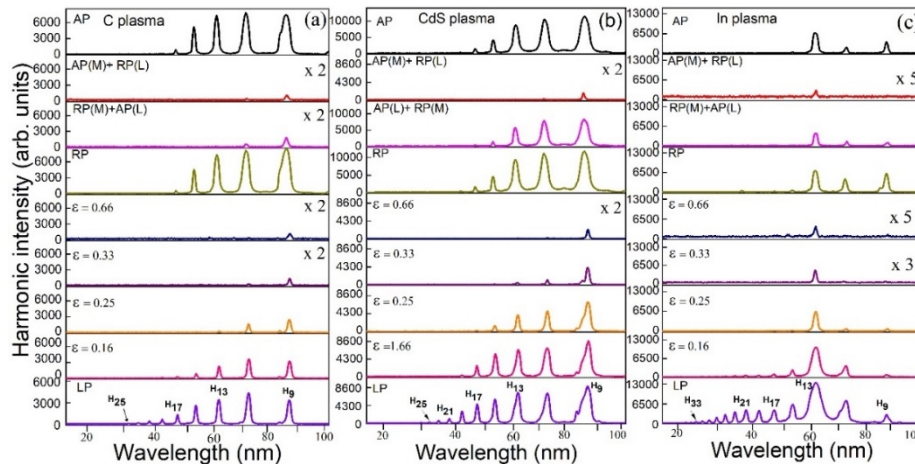

Fig. 2. Harmonics generation from different plasmas using different polarization states of the driving pulses. (a) C plasma. (b) CdS plasma. (c) In plasma. ε corresponds to the laser ellipticity. LP: linear polarization, AP: azimuthal polarization, RP: radial polarization, RP(M/L)+AP(L/M): superposition of laser polarizations having more radial and less azimuthal components and vice versa

Figures 2(a) and 2(b) show the harmonic spectra from C and CdS plasmas at different state of polarizations of driving pulses. As it was mentioned, the 2D color plots of harmonic spectra from C are depicted in Fig. 1(d) for better viewing of the divergence and respective intensities of high-order harmonics for different state of polarizations. The generated low-order harmonics

(9H-13H) using vector beams (RP and AP) are stronger compared to those produced by LP driving pulses. Below we analyze this effect in the frames of the phase-matching conditions.

Phase matching is one of the factors responsible for harmonic enhancement. Macroscopically, the harmonic efficiency depends on the interference of harmonics emitted from every atomic and ionic source. The constructive or destructive interference of harmonics depends on the harmonic phase. Quantitatively, the phase-matching depends on the length along which the emitted harmonics phases are identical, which will interfere constructively leading to harmonic enhancement. The phase matching can occur among the harmonics emitted from the atoms positioned in parallel and perpendicular polarizations with respect to the driving pulses propagation axis. The lengths along which harmonic phases are identical in perpendicular and parallel directions to the field axis are called transverse ($L_r^\perp$) and longitudinal (L_r^{II}) coherence lengths of harmonic r, which give rise to transverse and longitudinal phase-matching, respectively. They are defined as [38]

$$L_r^\perp = \pi / \Delta k_r^\perp \tag{1}$$

$$L_r^{||} = \pi / \Delta k_r^{||} \tag{2}$$

$$\Delta k_r^{||} \approx \frac{r\omega}{c}[\eta(r\omega) - \eta(\omega)] + \frac{\partial \xi(z)}{\partial z} + \alpha_r \frac{\partial I}{\partial z} \tag{3}$$

$$\Delta k_r^\perp \approx \frac{r\omega}{c}[-\eta(\omega)]\frac{\rho}{R(z)} + \alpha_r \frac{\partial I}{\partial \rho} \tag{4}$$

Here r is the harmonic order and $R(z)$ is the radius of curvature of the laser beam. The $\Delta k_r^{\perp \text{ or } ||}$ are the transverse or longitudinal phase mismatches, which depend on the Gouy phase (ξ), refractive index (η), the absorption coefficient of the medium at the specific harmonic order (α_r), intensity (I), and frequency (ω) of driving pulses. ρ and z represent the directions parallel and perpendicular to the driving pulses propagation axis, respectively. If considering the same laser parameters in vector and LP beams, longitudinal phase mismatch depends only on the Gouy phase ξ. The latter parameter is negligible for pure vector beams and selected laser parameters for LP beam [38,44].

Our laser parameters did not coincide with the properties of the fundamental beam specified in those studies. As a result, the effect of ξ is considerable in the case of the harmonics driven by LP Gaussian beams, which leads to phase mismatch. On one hand, in low density gases, the refractive index effects in HHG can be neglected. On other hand, the plasma densities from solids are considered high compared to gases, hence the refractive index can play important role in HHG. The heating pulse intensities utilized in our experiments are identical at the various polarization states of the driving pulses. Therefore, the effect of the refractive index on HHG is similar in our comparative studies using different polarization states. Overall, the negligible ξ in RP and AP beams leads to better longitudinal phase matching resulting in enhanced harmonic yields in the case of those beams compared with LP beam.

The transversal phase mismatch depends on the transversal phase (first term in Eq. (4)) and intrinsic phase ($\sim \alpha_r I$). The intrinsic phase depends on the laser parameters, which were identical in HHG studies with various polarized driving pulses. Transversal phase polarity (i.e. sign) depends on R, which is approximately the same for vector and LP beams. However, transversal phase mismatch contribution is negligible in the case of the vector beams having electric field vectors at the same/constant phase across the beam cross-section. The quantum numerical simulations of HHG driven by vector beams resulting in 5 times enhanced harmonic efficiency compared to LP beams, which was attributed to the transverse phase matching, are presented in Ref. [30]. They concluded that the effective source volume available with vector beams is greater than in the case of the Gaussian mode. Thus, the stronger harmonic generation with AP and RP beams as compared to LP beams can be attributed to greater longitudinal and transverse

phase matching due to the negligible Gouy phase variations, minimal transverse mismatch, and greater effective source volume.

Harmonic cut-offs from In, CdS, and C laser-induced plasmas in the case of the AP and RP beams are extended to 21H (32.5 eV), 19H (29.45 eV) and 17H (26.3 eV), respectively. Thus, the cut-off energies are reduced in the case of radial and azimuthal polarization of laser radiation as compared to LP beams. According to the cut-off law, the maximum harmonic cut-off energy $E_c = I_p + 3.17\, U_p$ where I_p is the ionization potential of generating medium and U_p is the ponderomotive potential defined as $U_p = 9.33 \times 10^{-14}\, I\lambda^2$ [W cm^{-2} µm^{-2}]. Correspondingly, harmonic cut-off depends on laser intensity (I) at focus and wavelength (λ) of driving pulses. Hence, identical intensities must be used for comparative studies. Notice that the vector beams need 2.7 times larger energy compared with the LP Gaussian beam to have the same peak intensity [30].

The used AR-coated S-waveplate, in accordance with the specification of the manufacturer, has very large (>99%) transmission at 800 nm. So the experiments with and without S-waveplate were carried out at approximately similar energies of the laser beams interacting with the laser-induced plasmas. There could be the difference in the intensities of the focused Gaussian and doughnut-like beams used in the case of waveplate-free experiments and application of waveplate, respectively. It is hard to distinguish a difference in the intensities of the focused radiation of different intensity distribution. By any means the intensity of the focused beam after propagation of the S-waveplate was not larger than the one of the focused Gaussian beam. Even at these, to some extent, less favorable conditions, the harmonic yield in the former case was larger compared with the latter case. This assumption confirms the advanced properties of the used vector beams. The reduced cut-offs with AP and RP beams might be attributed to the difference in the effective focused driving pulses intensities compared to LP light and the explanation given above [30].

Although the observed lower-order (9H) harmonic intensity with AP and RP beams is approximately 1.5- 2 times larger compared to LP beams (Fig. 3(a)), the observed intensity rate is less compared to the numerical estimates reported in [30]. The difference in numerical [30] and our experimental results might be related to the different intensities of focused LP, AP, and RP beams.
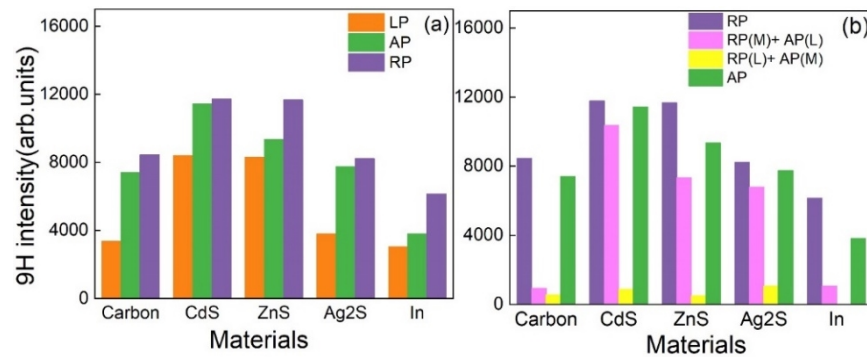

Fig. 3. Dependence of the 9H yield on the driving pulse polarization for different materials. (a) LP: linear polarization, AP: azimuthal polarization, RP: radial polarization. (b) RP(M/L)+AP(L/M): superposition of laser polarizations having more (M) radial and less (L) azimuthal components and vice versa.

Notice that the harmonic bandwidth is larger with RP and AP driving pulses compared with LP beams (Figs. 1(d) and 2). Overall, the AP and RP beams produced intense coherent extreme

ultraviolet beams with a wider bandwidth. The latter feature can lead to the smaller pulse width of generated harmonics.

The bar diagrams in Fig. 3(a) represent the 9H yield produced from C, CdS, ZnS, Ag$_2$S, and In plasmas by irradiating with AP, RP, and LP driving pulses. Table 1 comprises the harmonic intensity ratios of AP/LP and RP/LP driving pulses in the case of different laser-induced plasmas.

Table 1. 9th to 13th harmonic intensity ratios in the case of the AP, RP, and LP driving pulses propagating through the laser-induced plasmas of various materials (AP: azimuthal polarization, RP: radial polarization, LP: linear polarization)

Sample	LP/LP Harmonic intensity			RP/LP Harmonic intensity			AP/LP Harmonic intensity		
	9th	11th	13th	9th	11th	13th	9th	11th	13th
Carbon	1	1	1	2.5	1.9	2.1	2.2	1.8	2.1
CdS	1	1	1	1.4	1.6	1.4	1.4	1.4	1.3
ZnS	1	1	1	1.4	2.1	1.4	1.1	2.0	1.3
Ag2S	1	1	1	2.2	1.2	0.9	2.0	1.3	0.7
In	1	1	1	2.0	0.8	0.5	1.2	0.7	0.5

3.2. Resonance harmonic generation using vector and LP beams

The generation of narrowband intense single extreme ultraviolet wavelength via HHG has promising applications in the fields like imaging (i.e. with nanoscale resolutions) and spectroscopy. The specific extreme ultraviolet harmonic filters/gratings are needed to isolate the individual harmonics from the harmonic bunch generated by HHG. Alternatively, the resonant harmonic generation from laser-induced plasmas during HHG bypasses, to some extent, the necessity in filtering/separation. The resonant harmonic generation is well explained using the four-step model, wherein ejected and subsequently accelerated electron is trapped into an autoionizing state of ion and then decayed into the ground state while emitting the resonant harmonic. laser-induced plasmas containing In II ion allows the generation of a resonant harmonic close to the 62.1 nm (~19.92 eV), which corresponds to the radiative transition ($4d^{10}\ 5s^2\ ^1S_0$ - $4d^9\ 5s^2\ 5p\ (^2D)\ ^1P_1$) possessing large oscillator strength ($gf = 1.11$). Furthermore, resonant harmonic efficiency is notably higher than the efficiency of other neighboring harmonics [6].

Higher harmonics are generated by an atomic dipole or atomic transitions in the presence of intense laser field i.e. by electric field - atomic interactions. The harmonic generation is affected by electric dipole interaction which depends on the orientation of electric field with respect to atomic dipole, thus affecting the strengths and selection rules of transition. Therefore, spatially or temporally varying light polarization modifies the atomic transitions, which affects the higher harmonics.

In addition, it is well known that the vector beams have distinctive properties that alter the way of interaction with matter compared to the spatially homogenous beams. Our aim was to study the effect of vector beams on the resonant radiative transition by interacting with the indium laser-induced plasmas allowing the emission of resonant harmonic. The spectra of harmonics obtained from In plasma at various state of polarization of driving pulses are shown in Fig. 2(c). The employed 800 nm driving laser wavelength generates an intense 13th harmonic at ∼ 61.5 nm, i.e. close to the strong ionic transition of In II. The resonant harmonic generated with the LP beam was ~10 times stronger compared to the 9H and 17H. In addition, resonant harmonic intensity with LP driving pulses was approximately two times higher compared with the case when we used the AP and RP driving pulses. Thus our study showed that the application of vector beams resulted in less intense resonant harmonic, which indicates that those beams affect the spectroscopic properties of atoms and ions during laser-matter interaction.

The interaction of AP and RP beams with matter results in an alternation of the selection rules of transitions, which subsequently affects the electron movement in the atom leading to the increase of the probability of the transitions between the forbidden states [45–49]. It was clearly demonstrated in [47,49] that vector structured light excites the dipole forbidden modes of nano-oligomers and gold nanoparticle dimers by optical transitions having particularly modified transition selection rules. In addition, results of [46] also proved that RP and AP light excitation results in different selection rules, which lead to spin-flip transitions like spin-position entanglement and spin current injection in quantum dots. The monolayers of WSe_2 2D semiconductors generated the structured light from its spin-forbidden dark excitons [47].

Hence, the decreased resonance harmonic intensity can be attributed to the modification in the selection rules affected by spatially variable polarization of vector beams, which may reduce the *gf* of resonance transition from the autoionizing state to the ground state. HHG with vortex beams carrying topological charge 1, which produced ~50% reduced resonant harmonic intensity, was reported in [33]. They also interpreted this effect as a result of reduction of the oscillator strength of the transition responsible for the harmonic enhancement by modification in the selection rules of transition. In contrast, RP and AP beams generated intense 9H harmonic from In plasma with regard to the LP driving pulses, which was attributed to the enhanced phase matching, similarly to the CdS and C laser-induced plasmas cases (Figs. 2(c) and 3(a)).

3.3. Application of superposition of AP and RP beams for HHG in laser-induced plasmas

The illumination of materials with AP and RP superposition excites different modes simultaneously because of having strong longitudinal components of the magnetic and electric fields, respectively. The application of AP, RP, and their superposition's influencing the harmonic intensity and cut-off produced from C, CdS, and In laser-induced plasmas is shown in Figs. 2(a)–2(c). In the legends to those figures, AP(M/L) + RP(L/M) represent the superposition having more azimuthal and less radial components and vice versa respectively (i.e. M refers to more part of component and L corresponds to less part of component). Harmonic intensities are slightly greater from the RP beam compared to the AP beam while, as mentioned, harmonic cut-offs in these two cases are approximately the same, i.e. 17H for C laser-induced plasmas, 19H for CdS laser-induced plasmas, and 21H for In laser-induced plasmas. The slightly larger yield of harmonics in the case of the former beam might be due to the presence of the longitudinal electric component in the RP beam whereas it is zero in the case of the AP beam [50].

In recent reports, the enhanced second and third harmonics were generated using tightly focused RP beam compared with AP beam, which was explained by the presence of the stronger longitudinal electric field component in the former case [29,39]. However, in our case, the harmonic intensity ratios of AP/LP and RP/LP were approximately the same as shown in Table 1. Hence, one can assume that the AP and RP driving pulses produce bright extreme ultraviolet beams with approximately equal intensity. Meanwhile, the superposition of vector beams [AP(M/L)+ RP(L/M)] generates less intense and lower cut-off harmonics compared with LP, RP, and AP driving pulses (Figs. 1(d), 2, and 3(b)).

The macroscopic description of HHG points out that the harmonic efficiency depends on the interference of the phases of emitted harmonics from atoms and ions. RP and AP beams have the radial and azimuthal electric vector directions with π/2 phase difference between them. Hence, the reduced harmonic intensity with superposition is directly related to different harmonic interferences having phases orthogonal to each other. However, the superposition having more radial components generates higher cut-off and stronger extreme ultraviolet beams compared with the beam polarization having more azimuthal components.

The cut-offs with more radial components are extended up to 11H from C laser-induced plasmas and 17H from CdS laser-induced plasmas, whereas from more azimuthal components

those are 9H and 11H from the corresponding laser-induced plasmas. On another hand, the In laser-induced plasmas generated cut-off up to 13H with more radial components while with more azimuthal components we observed only resonant harmonic. This result again confirms that RP beams generate stronger harmonics compared with AP beams due to the presence of the longitudinal electric field components. Figure 3(b) shows the effect of vector beams and their superposition on 9H yield emitted from different laser-induced plasmas. The typical values of various harmonics enhancement ratios (i.e. superposition/RP) from different materials are presented in Table 2.

Table 2. Harmonic intensity ratios of [RP (M/L) +AP (L/M)]/RP measured in different laser-induced plasmas

Sample	RP/RP intensity	Harmonic		[RP(M)+AP(L)]/RP			[RP(L)+AP(M)]/RP		
				Harmonic intensity			Harmonic intensity		
	9th	11th	13th	9th	11th	13th	9th	11th	13th
Carbon	1	1	1	0.1	0.04	0	0.07	0.03	0
CdS	1	1	1	0.7	0.07	0.6	0.07	0.02	0
ZnS	1	1	1	0.6	0.5	0.4	0.04	0	0
Ag2S	1	1	1	0.8	0.7	0.4	0.12	0.04	0
In	1	1	1	0.2	0.3	0.6	0	0	0.1

3.4. Effect of driving pulse ellipticity on HHG

The impact of the polarization ellipticity (ε) of driving pulses on harmonic yield and the cut-off are shown in Figs. 4(a) and 4(b). Generally, the electric field ratio of two mutually perpendicular polarization components present in light is coined as ε. As depicted from the results shown in Fig. 4, the harmonic intensity and cut-off decrease with increasing ε due to a decrease in density of electrons recombining with their parent ions. Meanwhile, as it was mentioned, there is a need in the generation of stronger harmonics having elliptical polarization. The generation of resonant harmonic from laser-induced plasmas using the driving pulses with various ε can be considered as one of the solutions.

The influence of the fundamental pulse ε on the resonant harmonic at 62.2 nm (13H) from In II is shown in Fig. 4(c). Here we define the threshold ellipticity (ε_{th}) as the half-width at the half maximum of Gaussian fit applied to the particular (i.e. 9H, 11H, etc.) harmonic yield obtained at different DP ellipticities. It specifies the ε value where the harmonic yield is 50% of the yield produced with the light having zero ε.

The ε_{th} values are decreasing with harmonic order, according to the rules of electron re-collision in classical mechanics. However, the ε_{th} value of resonant harmonic from In laser-induced plasmas is deviating from the general trend. It shows less rapid decay of harmonic intensity compared to the rest of the harmonics. Microscopically, the electron recombination during HHG in the case of the driving pulses having different ellipticities depends on the electron trajectory and spatial extent of the recombination process. The less rapid decay of resonant harmonic might be due to the availability of some autoionizing states having larger wave function, which leads to a higher recombination probability between the returning electron and that state [51]. This means that the resonant harmonic intensity is decreasing slowly with the increase of driving pulse ellipticity as compared to the non-resonant harmonic intensity. Thus, the resonant harmonic intensity becomes higher compared to the non-resonant harmonics with increasing of the driving pulse ellipticity.

One of the ways to modify or control the polarization of extreme ultraviolet beams generated via HHG is by using the driving pulses of varying polarization. Particularly, laser ellipticity
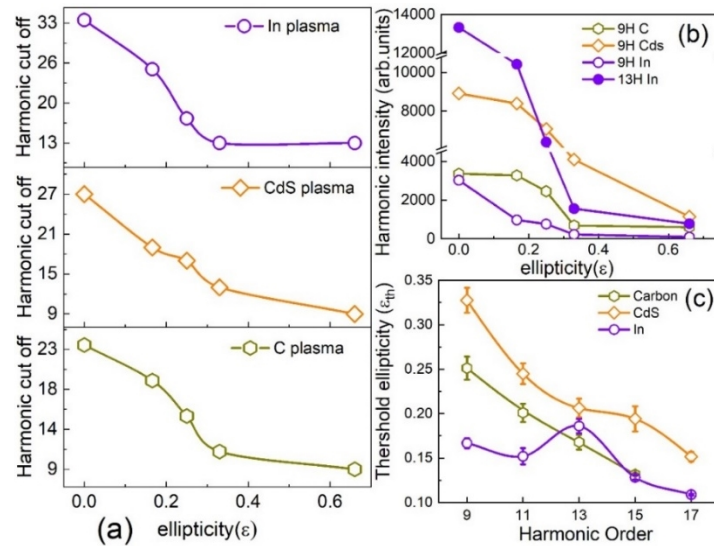
Fig. 4. (a) Harmonic cut-off and (b) harmonic intensity at different ellipticities (ε) of the polarization of the driving pulses. (c) Threshold ellipticity (εth) as a function of the harmonic order generated in different laser-induced plasmas.

allows generating the harmonics with elliptical polarization. However, the change in the ellipticity of fundamental beam from linear to elliptical or circular polarization drastically affects the harmonic yield becoming close to zero for the circular polarization due to a significant decrease of the recombination cross-section of the accelerated electrons with the parent ion. Therefore, the generating resonant harmonic at various ellipticity values of driving pulses becomes relatively stronger compared to the non-resonant harmonic.

Recently, the analytical model to reveal the mechanism responsible for the anomalous behavior of resonant harmonic with ellipticity was reported [52]. This model suggests that the electron recombining with parent ion after ionization by driving pulses of varying ellipticity is trapped into the autoionizing at higher probability in the case of the conditions of the resonance harmonic compared to the non-resonant case and then combines into the ground state. In addition, their results disclose that the resonant harmonics have polarization of higher ellipticity, which leads to the generation of the intense elliptically polarized harmonics.

As we underlined, our study provides the way to generate intense 13th resonant harmonic compared to the non-resonant harmonics while having different ellipticity by shaping the driving pulse polarization. Thus, modification of ε allows the formation of almost a single (resonant) harmonic yield during HHG, when other harmonics entirely disappear without the additional filtering of the coherent XUV output.

4. Conclusions

We generated the intense coherent extreme ultraviolet beams from the laser-induced plasmas containing CdS, ZnS, Ag_2S, C, and In by using the spatially structured polarization of the DPs and investigated the characteristics of high-order harmonics by modulating the polarization properties of driving pulses. The RP and AP beams generated ∼ 1.5 to 2 times stronger coherent extreme ultraviolet emission compared to the LP beams. The harmonic enhancement was attributed to the increase in transversal and longitudinal phase matching of generating high-order harmonics with RP and AP beams due to negligible Gouy phase, greater effective source volume, and minimal transverse mismatch. On the other hand, the resonant harmonic generating in indium

plasma using RP and AP beams was twice weaker than the one produced by LP light. The vector beams modify the selection rules of transitions, which reduce the oscillator strength of resonance transition and lead to reduced resonant harmonic intensity. Further, the AP + RP superposition's generated less intense harmonics with regard to AP and RP beams due to the destructive interference of harmonics having π/2 phase difference. RP beams and superposition with more radial components produced stronger harmonics compared to their counterparts (AP beams and superposition with more azimuthal components) due to the presence of the longitudinal electric field in the former case. Finally, we also demonstrated the effect of DP ellipticity on harmonic intensity and cut-off. CdS laser-induced plasmas allowed the generation of stronger harmonics compared with C and In laser-induced plasmas, with the exception of resonant harmonic in the latter case. The resonant harmonic intensity has less rapid decay with the growth of ellipticity compared to other harmonics due to the larger wave function of autoionizing state leading to better recombination with an accelerated electron during HHG. This experimental work provides a way to use different types of spatially structured laser beam polarization for HHG in different plasmas, which can find applications in spectroscopy, imaging, material science, etc.

References

1. T. Pfeifer, C. Spielmann, and G. Gerber, "Femtosecond x-ray science," Rep. Prog. Phys. **69**(2), 443–505 (2006).
2. F. Krausz and M. Ivanov, "Attosecond physics," Rev. Mod. Phys. **81**(1), 163–234 (2009).
3. R. Geneaux, H. J. B. Marroux, A. Guggenmos, D. M. Neumark, and S. R. Leone, "Transient absorption spectroscopy using high harmonic generation: a review of ultrafast X-ray dynamics in molecules and solids," Phil. Trans. R. Soc. A. **377**(2145), 20170463 (2019).
4. R. A. Ganeev, M. Suzuki, M. Baba, and H. Kuroda, "Harmonic generation in XUV from chromium plasma," Appl. Phys. Lett. **86**(13), 131116 (2005).
5. G. S. Boltaev, M. Iqbal, N. A. Abbasi, V. V. Kim, R. A. Ganeev, and A. S. Alnaser, "Enhanced XUV harmonics generation from diatomic gases using two orthogonally polarized laser fields," Sci. Rep. **11**(1), 5534 (2021).
6. T. Ozaki, L. B. Elouga Bom, R. Ganeev, J.-C. Kieffer, M. Suzuki, and H. Kuroda, "Intense harmonic generation from silver ablation," Laser Part. Beams **25**(2), 321–325 (2007).
7. M. A. Fareed, V. V. Strelkov, M. Singh, N. Thire, S. Mondal, B. E. Schmidt, F. Legare, and T. Ozaki, "Harmonic generation from neutral manganese atoms in the vicinity of the giant autoionization resonance," Phys. Rev. Lett. **121**(2), 023201 (2018).
8. R. A. Ganeev, "Generation of high-order harmonics of high-power lasers in plasmas produced under irradiation of solid target surfaces by a prepulse," Phys.-Usp. **52**(1), 55–77 (2009).
9. C. Hutchison, R. A. Ganeev, T. Witting, F. Frank, W. A. Okell, J. W. G. Tisch, and J. P. Marangos, "Stable generation of high-order harmonics of femtosecond laser radiation from laser produced plasma plumes at 1 kHz pulse repetition rate," Opt. Lett. **37**(11), 2064–2066 (2012).
10. N. Rosenthal and G. Marcus, "Discriminating between the role of phase matching and that of the single-atom response in resonance plasma-plume high-order harmonic generation," Phys. Rev. Lett. **115**(13), 133901 (2015).
11. M. Venkatesh, R. A. Ganeev, D. S. Ivanov, G. S. Boltaev, V. V. Kim, J. Liang, A. A. Samokhvalov, A. V. Kabashin, S. M. Klimentov, M. E. Garcia, and C. Guo, "High-order harmonic generation in Au nanoparticle-contained plasmas," Nanomaterials **10**(2), 234 (2020).
12. R. A. Ganeev, L. B. Elouga Bom, M. C. H. Wong, J.-P. Brichta, V. R. Bhardwaj, P. V. Redkin, and T. Ozaki, "High-order harmonic generation from C_{60}-rich plasma," Phys. Rev. A **80**(4), 043808 (2009).
13. J. Rothhardt, S. Hadrich, S. Demmler, M. Krebs, S. Fritzsche, J. Limpert, and A. Tunnermann, "Enhancing the macroscopic yield of narrow-band high-order harmonic generation by Fano resonances," Phys. Rev. Lett. **112**(23), 233002 (2014).
14. G. S. Boltaev, R. A. Ganeev, V. V. Strelkov, V. V. Kim, K. Zhang, M. Venkatesh, and C. Guo, "Resonance-enhanced harmonics in mixed laser-produced plasmas," Plasma Res. Express **1**(3), 035002 (2019).
15. M. A. Fareed, V. V. Strelkov, N. Thire, S. Mondal, B. E. Schmidt, F. Legare, and T. Ozaki, "High-order harmonic generation from the dressed autoionizing states," Nat. Commun. **8**(1), 16061–16065 (2017).
16. G. Tallents, E. Wagenaars, and G. Pert, "Lithography at EUV wavelengths," Nat. Photonics **4**(12), 809–811 (2010).

17. R. M. Kerber, J. M. Fitzgerald, S. S. Oh, D. E. Reiter, and O. Hess, "Orbital angular momentum dichroism in nanoantennas," Commun. Phys. **1**(1), 87–97 (2018).

18. C. Guclu, M. Veysi, and F. Capolino, "Photoinduced magnetic nanoprobe excited by an azimuthally polarized vector beam," ACS Photonics **3**(11), 2049–2058 (2016).

19. J. Miao, T. Ishikawa, I. K. Robinson, and M. M. Murnane, "Beyond crystallography: Diffractive imaging using coherent x-ray light sources," Science **348**(6234), 530–535 (2015).

20. O. Kfir, P. Grychtol, E. Turgut, R. Knut, D. Zusin, D. Popmintchev, T. Popmintchev, H. Nembach, J. M. Shaw, A. Fleischer, H. Kapteyn, M. Murnane, and O. Cohen, "Generation of bright phase-matched circularly-polarized extreme ultraviolet high harmonics," Nat. Photonics **9**(2), 99–105 (2015).

21. A. Fleischer, O. Kfir, T. Diskin, P. Sidorenko, and O. Cohen, "Spin angular momentum and tunable polarization in high-harmonic generation," Nat. Photonics **8**(7), 543–549 (2014).

22. T. Fan, P. Grychtol, R. Knut, C. Hernandez-Garcia, D. D. Hickstein, D. Zusin, C. Gentry, F. J. Dollar, C. A. Mancuso, C. W. Hogle, O. Kfir, D. Legut, K. Carva, J. L. Ellis, K. Dorney, C. Chen, O. Shpyrko, E. E. Fullerton, O. Cohen, P. M. Oppeneer, D. B. Milošević, A. Becker, A. A. Jaroń-Becker, T. Popmintchev, M. M. Murnane, and H. C. Kapteyn, "Bright circularly polarized soft X-ray high harmonics for X-ray magnetic circular dichroism," Proc. Natl. Acad. Sci. U.S.A. **112**(46), 14206–14211 (2015).

23. D. D. Hickstein, F. J. Dollar, P. Grychtol, J. L. Ellis, R. Knut, C. Hernández-García, D. Zusin, C. Gentry, J. M. Shaw, T. Fan, K. M. Dorney, A. Becker, A. Jaron-Becker, H. C. Kapteyn, M. M. Murnane, and C. G. Durfee, "Non-collinear generation of angularly isolated circularly polarized high harmonics," Nat. Photonics **9**(11), 743–750 (2015).

24. L. Medisauskas, J. Wragg, H. van der Hart, and M. Y. Ivanov, "Generating isolated elliptically polarized attosecond pulses using bichromatic counter rotating circularly polarized laser fields," Phys. Rev. Lett. **115**(15), 153001 (2015).

25. C. Hernández-García, C. G. Durfee, D. D. Hickstein, T. Popmintchev, A. Meier, M. M. Murnane, H. C. Kapteyn, I. J. Sola, A. Jaron-Becker, and A. Becker, "Schemes for generation of isolated attosecond pulses of pure circular polarization," Phys. Rev. A **93**(4), 043855 (2016).

26. P.-C. Huang, C. Hernández-García, J.-T. Huang, P.-Y. Huang, C.-H. Lu, L. Rego, D. D. Hickstein, J. L. Ellis, A. Jaron-Becker, A. Becker, S.-D. Yang, C. G. Durfee, L. Plaja, H. C. Kapteyn, M. M. Murnane, A. H. Kung, and M.-C. Chen, "Polarization control of isolated high-harmonic pulses," Nat. Photonics **12**(6), 349–354 (2018).

27. F. Kong, C. Zhang, H. Larocque, Z. Li, F. Bouchard, D. H. Ko, G. G. Brown, A. Korobenko, T. J. Hammond, R. W. Boyd, E. Karimi, and P. B. Corkum, "Vectorizing the spatial structure of high-harmonic radiation from gas," Nat. Commun. **10**(1), 2020 (2019).

28. J. Wätzel and J. Berakdar, "Multipolar, polarization-shaped high-order harmonic generation by intense vector beams," Phys. Rev. A **101**(4), 043409 (2020).

29. Z.-Y. Chen and R. Hu, "Intense high-order harmonic vector beams from relativistic plasma mirrors," Phys. Rev. A **103**(2), 023507 (2021).

30. C. Hernández-García, A. Turpin, J. San Román, A. Picón, R. Drevinskas, A. Cerkauskaite, P. G. Kazansky, C. G. Durfee, and ÍJ Sola, "Extreme ultraviolet vector beams driven by infrared lasers," Optica **4**(5), 520–526 (2017).

31. N. Zaïm, D. Guénot, L. Chopineau, A. Denoeud, O. Lundh, H. Vincenti, F. Quéré, and J. Faure, "Interaction of ultraintense radially-polarized laser pulses with plasma mirrors," Phys. Rev. X **10**(4), 041064 (2020).

32. M. Suzuki, M. Baba, R. Ganeev, H. Kuroda, and T. Ozaki, "Anomalous enhancement of a single high-order harmonic by using a laser-ablation tin plume at 47 nm," Opt. Lett. **31**(22), 3306–3308 (2006).

33. M. Singh, M. A. Fareed, A. Laramée, E. Isgandarov, and T. Ozaki, "Intense vortex high-order harmonics generated from laser-ablated plume," Appl. Phys. Lett. **115**(23), 231105 (2019).

34. R. Drevinskas, J. Zhang, M. Beresna, M. Gecevičius, A. G. Kazanskii, Y. P. Svirko, and P. G. Kazansky, "Laser material processing with tightly focused cylindrical vector beams," Appl. Phys. Lett. **108**(22), 221107 (2016).

35. C. Hnatovsky, V. Shvedov, W. Krolikowski, and A. Rode, "Revealing local field structure of focused ultrashort pulses," Phys. Rev. Lett. **106**(12), 123901 (2011).

36. Y. I. Salamin, Z. Harman, and C. H. Keitel, "Direct high-power laser acceleration of ions for medical applications," Phys. Rev. Lett. **100**(15), 155004 (2008).

37. B. S. Bhargava Ram, P. Senthilkumaran, and A. Sharma, "Polarization-based spatial filtering for directional and nondirectional edge enhancement using an S-waveplate," Appl. Opt. **56**(11), 3171–3178 (2017).

38. C. Hernández-García, I. J. Sola, and L. Plaja, "Signature of the transversal coherence length in high-order harmonic generation," Phys. Rev. A **88**(4), 043848 (2013).

39. R. Camacho-Morales, G. Bautista, X. Zang, L. Xu, L. Turquet, A. Miroshnichenko, H. H. Tan, A. Lamprianidis, M. Rahmani, C. Jagadish, D. N. Neshev, and M. Kauranen, "Resonant harmonic generation in AlGaAs nanoantennas probed by cylindrical vector beams," Nanoscale **11**(4), 1745–1753 (2019).

40. G. Bautista, J. Makitalo, Y. Chen, V. Dhaka, M. Grasso, L. Karvonen, H. Jiang, M. J. Huttunen, T. Huhtio, H. Lipsanen, and M. Kauranen, "Second-harmonic generation imaging of semiconductor nanowires with focused vector beams," Nano Lett. **15**(3), 1564–1569 (2015).

41. R. A. Ganeev, M. Suzuki, S. Yoneya, and H. Kuroda, "High-order harmonic generation during propagation of femtosecond pulses through the laser-produced plasmas of semiconductors," J. Appl. Phys. **117**(2), 023114 (2015).

42. R. A. Ganeev, T. Witting, C. Hutchison, V. V. Strelkov, F. Frank, M. Castillejo, I. Lopez-Quintas, Z. Abdelrahman, J. W. G. Tisch, and J. P. Marangos, "Comparative studies of resonance enhancement of harmonic radiation in indium plasma using multicycle and few-cycle pulses," Phys. Rev. A **88**(3), 033838 (2013).

43. M. R. Vázquez, B. Sotillo, S. Rampini, V. Bharadwaj, B. Gholipour, P. Fernández, R. Ramponi, C. Soci, and S. M. Eaton, "Femtosecond laser inscription of nonlinear photonic circuits in Gallium Lanthanum Sulphide glass," J. Phys. Photonics **1**(1), 015006 (2018).

44. M. M. Sanchez-Lopez, J. A. Davis, I. Moreno, A. Cofre, and D. M. Cottrell, "Gouy phase effects on propagation of pure and hybrid vector beams," Opt. Express **27**(3), 2374–2386 (2019).

45. S. Reich, N. S. Mueller, and M. Bubula, "Selection rules for structured light in nanooligomers and other nanosystems," ACS Photonics **7**(6), 1537–1550 (2020).

46. J. Wätzel, E. Y. Sherman, and J. Berakdar, "Nanostructures in structured light: Photoinduced spin and orbital electron dynamics," Phys. Rev. B **101**(23), 235304 (2020).

47. S. Borghardt, J. Sonntag, J.-S. Tu, T. Taniguchi, K. Watanabe, B. Beschoten, C. Stampfer, and B. Ewa Kardynał, "Radially polarized light beams from spin-forbidden dark excitons and trions in monolayer WSe2," Opt. Mater. Express **10**(5), 1273–1285 (2020).

48. J. Wang, F. Castellucci, and S. Franke-Arnold, "Vectorial light–matter interaction: Exploring spatially structured complex light fields," AVS Quantum Sci. **2**(3), 031702 (2020).

49. T. S. Deng, J. Parker, Y. Yifat, N. Shepherd, and N. F. Scherer, "Dark plasmon modes in symmetric gold nanoparticle dimers illuminated by focused cylindrical vector beams," J. Phys. Chem. C **122**(48), 27662–27672 (2018).

50. T. M. Jeong, S. Bulanov, S. Weber, and G. Korn, "Analysis on the longitudinal field strength formed by tightly-focused radially-polarized femtosecond petawatt laser pulse," Opt. Express **26**(25), 33091–33107 (2018).

51. Y. H. Lai, K. S. Rao, J. Liang, X. Wang, C. Guo, W. Yu, and W. Li, "Resonance-enhanced high harmonic in metal ions driven by elliptically polarized laser pulses," Opt. Lett. **46**(10), 2372–2375 (2021).

52. M. A. Khokhlova, M. Y. Emelin, M. Y. Ryabikin, and V. V. Strelkov, "Polarization control of quasimonochromatic XUV light produced via resonant high-order harmonic generation," Phys. Rev. A **103**(4), 043114 (2021).